Clays and Clay Minerals, Vol. 50, No. 5, 562–577, 2002.

THICKNESS DISTRIBUTION OF ILLITE CRYSTALS IN SHALES. I: X-RAY DIFFRACTION *VS.* HIGH-RESOLUTION TRANSMISSION ELECTRON MICROSCOPY MEASUREMENTS

TERESA DUDEK[1,*], JAN ŚRODOŃ[1], DENNIS D. EBERL[2], FRANÇOISE ELSASS[3] AND PETER UHLIK[4]

[1] Institute of Geological Sciences, Polish Academy of Sciences, Senacka 1, 31-002 Kraków, Poland
[2] US Geological Survey, Suite E-127, 3215 Marine St., Boulder, Colorado 80303-1066, USA
[3] Science du Sol INRA, Versailles, France
[4] Department of Mineral Deposits, Comenius University, Bratislava, Slovakia

Abstract—Two independent methods of crystal-size distribution analysis were compared: the Bertaut-Warren-Averbach XRD technique (MudMaster computer program) and high-resolution transmission electron microscopy (HRTEM). These techniques were used to measure thickness distributions of illite crystals (fundamental particles) from sets of illite-smectites from shales and bentonites that had expandabilities ranging from 86%S to 6%S. The illite-smectites were treated with a polymer (polyvinylopyrolidone, PVP) to separate them into fundamental particles for XRD and HRTEM investigations.

A systematic difference between XRD and HRTEM results was observed: XRD (area-weighted distributions) detected a larger fraction of thick (>4 nm) and a smaller fraction of thin crystals as compared to HRTEM (number-weighted distributions). As a result, XRD-determined distributions have larger mean thickness values and larger distribution parameters (α and β^2). The measurements performed by the two techniques were verified by modeling XRD patterns of the PVP-illites, using the measured distributions as inputs. The modeling indicated that the XRD-determined distributions are very accurate. Selecting broader thickness distributions in MudMaster further improved the modeling results. The HRTEM measurements underestimate the proportion of coarse particles, in particular in shale samples, and this inaccuracy is attributed to the effect of using number-weighted (rather than area-weighted) distributions and to inaccurate counting statistics for thick crystals.

Key Words—BWA Analysis, Crystal Size Distribution, Fundamental Particles, HRTEM, Illite-smectite, Lognormal Distribution, MudMaster, XRD.

INTRODUCTION

Crystal size and size distribution are essential characteristics of clay minerals. Determination of these parameters is becoming a powerful tool for understanding geological history (*e.g.* degree of diagenesis and low-grade metamorphism), crystal growth processes, and the technological properties of clay raw materials (*e.g.* Merriman *et al.*, 1990; Nieto and Sanchez-Navas, 1994; Eberl *et al.*, 1998a; Kile *et al.*, 2000; Środoń *et al.*, 2000). All of these applications require accurate and reproducible crystal-size measurements.

X-ray diffraction (XRD) and electron or atomic force microscopy (AFM) are the common techniques used to analyze the size of nano-crystals. The advantage of the microscopic methods is that objects can be observed directly. The disadvantage is that the measurements are time-consuming, expensive and may not be statistically satisfactory. X-ray diffraction techniques are based on the analysis of peak profiles of periodic crystals (*i.e.* the effect of interstratification on peak broadening has to be excluded prior to measurement). Three main effects contribute to broadening: (1) the mean size and size distribution of coherent X-ray scattering domains measured normal to the planes of diffraction; (2) fluctuations of the *d*-values (*i.e.* strain); and (3) instrumental effects. In contrast to the microscopic methods, the XRD technique is quick and statistically reliable, because the XRD peaks average diffraction effects from billions of individual crystals. A potential shortcoming of this technique is that the measured objects are coherent scattering domains, which may or may not be strictly equivalent to the microscopically observed crystals. Additionally, the XRD technique requires a theoretical treatment of the XRD patterns in order to extract information concerning coherent scattering domain size. This treatment is based on some assumptions and simplifications that may disturb the results.

There are several mathematical approaches to extract information on the size of coherent scattering domains from the XRD peak shape: the Scherrer equation (Drits *et al.*, 1997), the variance method of Wilson (1963 in Árkai *et al.*, 1996), the Voigt method (Langford (1978) in Árkai *et al.*, 1996), and the Bertaut-Warren-Averbach (BWA) method (Eberl *et al.*, 1996; Drits *et al.*, 1998). The BWA method is the most universal, because it measures mean size, size distribution and strain, in contrast to the other methods which yield information on mean size only (the Scherrer equation) or on mean size and strain (the variance and Voigt methods). Drits *et al.*

* E-mail address of corresponding author:
nddudek@cyf-kr.edu.pl

(1998) adapted the BWA method to clay studies, and developed the computer program named MudMaster (Eberl *et al.*, 1996). MudMaster was subsequently used by Eberl *et al.* (1998b) to calculate mean thicknesses ($\bar{T}$) and thickness distributions for coherent scattering domains for a series of diagenetic and hydrothermal bentonites. They showed that the resulting values of $\bar{T}$ were systematically slightly larger than the corresponding $\bar{T}$ values of crystals measured by the Pt-shadowing TEM technique. This result implied that coherent scattering domains are equivalent to crystals observed in TEM (there is no domain structure within crystals).

The present contribution follows the research of Drits *et al.* (1998) and Eberl *et al.* (1998a, 1998b) by extending the studies to the illitic material of shales. The reliability of two independent techniques used for assessing the size of clay crystals, XRD-BWA (MudMaster) and high-resolution transmission electron microscopy (HRTEM), is compared and evaluated. The measured objects are illite crystals and smectite monolayers from a set of shales, with a few bentonite samples used for reference. In the original samples, only some illite crystals occur independently (as discrete illite). Others, together with smectite monolayers, are building blocks of mixed-layer illite-smectite (I-S) crystals (fundamental particles *sensu* Nadeau *et al.*, 1984). They are kept delaminated (*i.e.* the effect of mixed-layering is removed) by using the procedure of sample saturation with polymer PVP according to the technique of Eberl *et al.* (1998b).

In a following paper (Dudek and Środoń, in review), the extracted crystal thickness distributions are analyzed and interpreted in terms of the mechanism of smectite illitization in shales.

MATERIALS

Three samples of bentonite-like clays and 13 samples of shales were selected for detailed studies (Table 1). For both rock types, the clay fraction (usually <0.2 μm) was analyzed. The following bentonite-like samples were investigated: RM30, a hydrothermal sericite (6%S) from the Silverton Caldera, Colorado, USA (Eberl *et al.*, 1987), M11, an I-S (6%S) from the Welsh Borderlands, UK (Środoń *et al.*, 1986), and the Zempleni I-S (16%S) from hydrothermally altered volcanics from Zempleni Hills in NE Hungary (Środoń, 1984).

The shale samples came from boreholes located in the Polish sector of flysch Carpathians (Kuźmina-1) and in the Polish (Jodłówka-4, Załazie-2, Ryszkowa Wola-1) and Ukrainian (Załużany) parts of the Carpathian Foredeep (Table 1). The shale samples selected from above and from within the zone of burial diagenesis, cover a wide range of expandabilities (from 86%S to 19%S), and have both R = 0 and R >0 ordering (Dudek, 2001).

The Carpathian Foredeep is a foreland basin supplied mainly by reworked flysch sediments from the Carpathians. The Carpathian rocks themselves were

Table 1. Verification of the PVP dispersion technique based on the positions of 00*l* reflections [d_{00l}] from PVP preparations, and of the recovered interference function [d_{00l}int] after MudMaster analysis. An integral series of reflections indicates proper dispersion (removal of mixed-layer diffraction effects). Also presented are expandability, ordering, the grain-size fraction and the composition of clay/PVP suspensions.

Sample	%S XRD, ordering	Fraction (μm)	Clay:PVP	d_{001}	d_{002}	d_{003}	d_{005}	d_{001}int
Carpathian shales								
Ku-80	40, R=0	<0.2	1 : 2	10.07	4.99	3.33	2.00	10.05
Ku-82	19, R=1	<0.2	1 : 2	10.09	4.97	3.32	2.00	9.96
Carpathian Foredeep shales (Poland)								
Jł4-13	46, R=0	<0.2	1 : 2	10.00	5.01	3.32	1.99	10.00
Jł4-16	55, R=0	<0.2	1 : 2	10.09	4.99	3.32	1.99	9.94
Jł4-17	36, R=1	<0.2	1 : 2	10.00	4.99	3.32	1.99	9.98
Zł2-6	67, R=0	<0.2	1 : 3	10.03	5.02	3.34	2.00	9.98
Zł2-9	47, R=0	<0.2	1 : 2	9.96	4.99	3.32	1.99	9.96
Zł2-12	44, R=0/1	<0.2	1 : 2	9.98	4.98	3.32	1.99	9.96
Zł2-14	42, R=0/1	<0.2	1 : 2	9.96	4.98	3.32	1.99	9.94
RW-1	86, R=0	<0.2	1 : 4	10.00	4.98	3.33	1.99	9.91
Carpathian Foredeep shales (Ukraine)								
Zy-28	30, R=1	<0.2	1 : 2	9.98	4.97	3.33	1.99	9.98
Zy-19	28, R=1	<0.2	1 : 2	10.00	4.98	3.32	1.99	9.94
Zy-14	29, R=1	<0.2	1 : 2	9.96	4.98	3.33	1.99	9.94
Bentonites								
RM30	6, R>1	<2	1 : 2	9.98	5.01	3.33	2.00	9.96
M11	6, R>1	<2	1 : 2	10.09	5.00	3.34	1.99	9.94
Zemp	16, R>1	<0.2	1 : 2	10.38	5.03	3.33	2.00	9.85

formed mainly as the product of density currents, the processes causing extensive homogenization and mixing of the material. It is expected that the two cycles of reworking would lead to a remarkable uniformity of the Carpathian Foredeep rocks, an assumption that is supported by whole-rock quantitative mineral analyses (Dudek, 2001). Therefore, in theoretical modeling of XRD patterns of illite performed in the present study, a unique chemical composition for illite was used (unique $Lp G^2$, see below).

EXPERIMENTAL

Preparation of PVP clays

Firstly, carbonates, Fe and Mn oxides, and organic matter were removed from the samples (Jackson, 1975), and the Na-saturated clay fraction was separated by centrifugation, followed by dialysis. Next, illite-smectites were separated into fundamental particles by dispersion in water, and then PVP-10 (polyvinylpyrrolidone, molecular weight 10,000) was added to keep the fundamental particles from reassociating on drying (Eberl *et al.*, 1998b). The XRD and HRTEM measurements were made on the same material.

The details of the technique used for PVP intercalation are as follows. The clay fraction of Na-saturated samples of shales and bentonites was suspended in distilled water (concentration 2.5 mg clay/1 mL H_2O), fully dispersed by ultrasonic treatment, and mixed with an appropriate amount of an aqueous solution containing 5 mg PVP/1 mL H_2O. The proportion of clay to PVP used depended on the expandability of the sample: the larger the proportion of smectite layers, the more PVP was added to obtain a good intercalation. Samples with expandabilities below 50%S were mixed in proportions of 5 mg PVP to 2.5 mg clay (1 mL PVP solution/mL clay suspension), whereas the amount of PVP added for clays >50%S was chosen by interpolation between the former proportion and that used for pure smectite (10 mg PVP to 2.5 mg clay, or 2 mL PVP solution/mL clay suspension; Table 1). The mixtures were shaken by hand, left for a few minutes, sonified at low power for ~10–15 s, and then mounted appropriately for XRD and HRTEM studies.

XRD measurements

The PVP-clay suspensions were dried at 60°C on Si single crystal, polished wafers that had been glued to standard glass slides (technique of Eberl *et al.*, 1998b). A Si wafer substrate produces low background and does not yield peaks that would interfere with illite peaks (only a weak but sharp peak at 33°2θ may be registered).

The XRD patterns were recorded at the USGS in Boulder, Colorado, using a Siemens D500 diffractometer equipped with a Cu tube, a graphite monochromator (necessary to obtain low XRD background intensities), a scintillation counter, and the following slit system between the tube and the detector: 1°, 1°, sample, Soller, 1°, 0.15°, 0.15°. Samples were analyzed from 2 to 50°2θ, with a step size of 0.02°2θ, and a count time of 5 s per step. The tube current and voltage were 30 mA and 40 kV, respectively.

Coherent scattering domain size analysis: BWA method and MudMaster computer program

The BWA technique, applied in the MudMaster computer program to calculate mean size, size distribution and microstrain in coherent scattering domains, is based on Fourier analysis of the interference function (Eberl *et al.*, 1996; Drits *et al.*, 1998). The analysis was limited to 00*l* diffraction peaks for illite, which record the thickness of coherent scattering domains.

The 001 illite basal reflection was analyzed for all samples. This reflection is most suitable for BWA analysis because, in contrast to the higher-order reflections, it is relatively intense and not influenced by strain broadening. Also, as was shown by Dudek (2001) using NEWMOD-calculated theoretical patterns of illite, MudMaster produces the most precise results from the 001 peak. In addition, the shape of the illite 001 reflection is least affected by the proximity of the chlorite peak (6.17°2θ), often present in shale samples. The 001 chlorite reflection can be removed by using the program PeakChopper (which is attached to the MudMaster package) prior to MudMaster analysis. The main disadvantage of using the 001 peak is that its shape is more affected by the $Lp G^2$ factor than are the shapes of higher-order reflections (Eberl *et al.*, 1998b). This disadvantage can be minimized by careful selection of the $Lp G^2$ factor. This factor for PVP-illite was calculated as recommended by Eberl *et al.* (1998b) using the weighted sum of a measured $Lp G^2$ for PVP-smectite (corresponding to the illite crystal basal surfaces), and of a theoretically calculated $Lp G^2$ for illite (the crystal interiors):

$$(Lp G^2)_{\text{PVP-illite}} = (1 - A)\,(Lp G^2)_{\text{PVP-smectite}} + A(Lp G^2)_{\text{illite}} \quad (1)$$

where $A = (\bar{T} - 1)/\bar{T}$

The settings recommended in the program (Eberl *et al.*, 1996) for the analysis of the 001 PVP-illite reflection were applied. The most important outputs of MudMaster are thickness distribution, mean thickness extrapolated from the Fourier coefficients (also called 'best mean'), mean thickness calculated from the distribution, mean of the logarithms of coherent scattering domain thickness (α), and variance of the logarithms of coherent scattering domain thickness (β^2). The mean thickness calculated from the distribution is strongly affected by the distribution upper limit, which must be chosen arbitrarily. Therefore, the extrapolated mean thickness was recommended by Eberl *et al.* (1996) as the best value, and the mean thickness from the distribution was made equal to it by adjusting the distribution limit. Two

Table 2. Steps of the procedure used to intercalate samples with PVP for HRTEM investigations.

Saturating liquid	No. of exchanges	Time	Temperature (°C)
100% methanol	4	1 h	20
2/3 methanol, 1/3 propylene oxide	1	15 min	20
1/2 methanol, 1/2 propylene oxide	1	15 min	20
1/3 methanol, 2/3 propylene oxide	1	15 min	20
100% propylene oxide	3	45 min	20
Resin, propylene oxide	1	12 h	20
Resin	1	3–4 h	20
Polymerization of resin		24 h	60

characteristics of BWA analysis have to be emphasized: (1) smectite monolayers are not detectable; therefore only illites can be measured; and (2) thickness distributions are area-weighted (*i.e.* the frequency of illites of a given thickness corresponds to normalized sums of <*ab*> areas of these illites).

The effects of factors other than coherent scattering domain size on peak broadening (Drits *et al.*, 1998) were minimized by selecting diagenetic samples with expected $\bar{T}$ <20 nm (the instrumental effects can be ignored), and by using the 001 reflection (the effect of strain can be ignored).

To check the reproducibility of PVP intercalation, PVP-XRD slides were prepared and analyzed twice. The differences between the two analyses were found to be negligible: 0.2 nm in the $\bar{T}$ value, 0.03 in α, and 0.04 in β[2].

HRTEM preparations

Approximately 2 mL of the PVP-clay suspension was poured onto Scotch tape (4 cm^2) that had been stuck to a glass slide (it is easier to remove a thin film of the sample from a Scotch tape than directly from glass) and dried at 60°C on a hot plate. A HRTEM specimen prepared in this way fulfils two criteria required in the present study: (1) the sample analyzed by HRTEM is as similar as possible to the sample analyzed by XRD; and (2) analyzed crystals are well oriented. A small amount of the sample (usually ~10 mm^2) is extracted from the Scotch tape and embedded in resin according to the procedure described below.

The method used to prepare PVP samples for HRTEM investigations was based on the technique of Spurr (1969), adapted by Tessier (1984) and Elsass *et al.* (1998) to study the fabric of soils. The following treatments were used (Table 2): a small piece of sample extracted from the Scotch tape was coated with 2% agar and dehydrated by exchanging water for methanol. Methanol was replaced in a step-like manner by propylene oxide (1,2-epoxypropane), and finally the sample was impregnated with the low-viscosity epoxy resin of Spurr (1969). If a thin film of sample was transparent (often the case because the sample/PVP mixture was very dilute), the specimen was carbon-coated prior to embedding it in the resin, because otherwise the sample might have been invisible in the resin. (This technique was developed independently of the technique of PVP-sample preparation for HRTEM investigations presented in Uhlik (1999) and Uhlik *et al.* (2000b). Both methods are similar, though the technique described in the present study is quicker: in order to locate easily a sample in the resin, Uhlik (1999) and Uhlik *et al.* (2000b) prepared a thick specimen film that takes about 2 days, in contrast to carbon coating of a thin-specimen film (30 min) applied in the present work.) The sample was then sliced into ultrathin sections with a diamond knife using the REICHERT ULTRACUT E microtome, and the sections were deposited on copper grids covered with collodion and carbon. The thickness of a slice usually exceeded 70 nm, because silicates are relatively hard and it is difficult to cut them into thinner sections.

Thirteen of the investigated PVP samples were imaged using a Philips 420 STEM microscope (INRA, Versailles). The remaining three samples were analyzed in a JEOL JEM-2000 FX microscope (Comenius University, Bratislava). The working parameters for the two instruments are presented in Table 3.

Table 3. Settings of HRTEM instruments used.

	Philips 420 STEM	JEOL JEM-2000 FX
Accelerating voltage	120 kV	160 kV
Objective aperture	40 μm	50 μm
Scherzer defocus	−150 nm	from −86 to −136 nm
Spherical aberration coefficient	2.65 mm	3.4 mm
Chromatic aberration coefficient	–	3.1 mm
Scherzer resolution	0.35 nm for line image	0.28 nm for line image 0.32 nm for point image

https://doi.org/10.1346/000986002320679305 Published online by Cambridge University Press

Method of HRTEM measurements and measurement error

At least 10 photographs of each sample were taken. Magnifications of 51000× in Versailles and 60000× in Bratislava were routinely applied. The number of layers in each crystal was counted directly on the negatives using a binocular microscope with a micrometric scale and magnifications of 15–40×. This detailed analysis was preceded by examination of the negatives on a light table in order to choose the best areas for observation and to exclude areas of the sample that had been photographed more than once. In the negatives, the silicate layers with high electrostatic potential appear white, and the interlayer spaces with low potential appear dark. One hundred and fifty measurements of crystals were regarded as statistically sufficient (Środoń *et al.*, 1990; Elsass *et al.*, 1998). To verify the measurements, the total crystal thickness for a number of crystals was measured between the centers of external layers. The value of interlayer spacing obtained by dividing the total thickness of the crystals by the number of interlayers ($n - 1$) was found to correspond to ~10 Å, *i.e.* the thickness of one illite layer. This result ensured the reliability of measurements by excluding the possibility of the presence of smectite interlayers in the measured crystals. Special attention was paid to recognize and to exclude pictures taken when the focus of the microscope was not set properly, *i.e.* when underfocus was too strong or when the microscope was overfocused. In both cases, artifacts are introduced to the images. When underfocus is too strong, the resolution is poor and bilayers could be mistaken for monolayers. This artifact could be easily recognized because lattice fringes are thick and blurred. In overfocus conditions, the contrast is reversed (interlayers are white and layers are dark) and in this case monolayers could be mistaken for bilayers. This artifact could be recognized by examining the external fringes of crystals, which, when the microscope is properly focused, should have edges darker than the resin in the background.

In each sample, the thicknesses of crystals, expressed as the number of layers (n) were determined, and the mean thickness, $\bar{T}$ was calculated according to:

$$\bar{T} = \frac{\sum_{i=1}^{n} x_i f(x)_i}{\sum_{i=1}^{n} f(x)_i} \qquad (2)$$

where x = thickness categories and $f(x)$ = the number of measured crystals in a given category.

The HRTEM measurements, in contrast to those by XRD, yield distributions for both illite plus smectite ('I+S') and for illite ('Illite') crystals. These distributions are number-weighted, because <*ab*> areas of crystals cannot be measured from HRTEM images. Number-weighted distributions correspond to the area-weighted distributions only if there is no functional relationship between area and thickness.

Calculation of theoretical XRD patterns of illite

The thickness distributions of illites measured by XRD and HRTEM methods were evaluated by simulating XRD tracings of PVP-illites using the measured distributions as the input. The program NEWMOD© (Reynolds, 1985) cannot be used in this case, because it does not include the effect of PVP on the diffraction patterns of illite. Instead, the following sequence of calculations was performed in Excel worksheets:

(1) The illite interference function (ϕ) was calculated using equation 3.15 from Moore and Reynolds (1997, p. 92, corrected by excluding N from the denominator) and applying the measured distributions.

(2) The layer scattering factor for illite (G^2) and the Lorentz-polarization factor (Lp) were calculated in the spreadsheet CALCLPG2.xls (part of the MudMaster package), which is based on the equations 3.9 and 3.13 from Moore and Reynolds (1997, pp. 88 and 90, respectively). LpG^2 for PVP-illite was then calculated using equation 1. The calculations were performed assuming an Fe-free illite structure (allowing 0.3 Fe atoms per half unit-cell for shale samples did not improved the fit).

(3) The diffraction function of PVP-illite was computed as a product of the interference function (ϕ) and the LpG^2 factor.

(4) Finally, the diffraction function was corrected for the intensity loss at low diffraction angles due to insufficient sample length (Moore and Reynolds 1997, p. 300).

The reliability of the calculations of illite XRD patterns was tested in two steps:

(1) First, a modified Scherrer equation was used, following the approach presented by Drits *et al.* (1997). This equation relates the mean thickness of coherent scattering domains to the shape of the interference function peaks. The equation, applied to the calculated illite patterns, should produce the same mean thickness values for all basal reflections, and this thickness should equal the mean thickness of the input distribution. Two interference functions for illite were tested. These distributions were lognormal with means of 5 nm and 10 nm. The lognormal distribution is characteristic of many bentonitic samples (Eberl *et al.*, 1998a; Środoń *et al.*, 2000). The calculated lognormal distributions were terminated at the maximum crystal thickness (T_{max}) = 5 × $\bar{T}$. The frequency of lognormal distribution for this T_{max} falls below 0.001 of the maximum frequency.

The mean volume-weighted thickness (L_{meas}) calculated using integral intensities of reflections (β_i) (equation 19 in Drits *et al.*, 1997), are essentially the same for all reflections in the two tested examples, indicating no angle-dependent error in the interference

https://doi.org/10.1346/000986002320679305 Published online by Cambridge University Press

function calculations (Table 4). L_{meas} closely matches the mean volume-weighted thicknesses calculated from the input distribution (L_{distr}) (equations 22 and 25 in Drits *et al.*, 1997). This match indicates that the Excel calculations of the interference function of illite are correct. L_{meas} was calculated using β_i measured by including all diffracted intensity chosen halfway between the °2θ values for the successive reflections. Ignoring the 'background' would result in underestimation of β_i and overestimation of L_{meas}. The latter effect was observed by Drits *et al.* (1997) for the NEWMOD© -calculated patterns of illite and was related to intensity loss during background removal, particularly for intensity contributions from the thinnest coherent scattering domains. Thin coherent scattering domains produce larger intensities farther from the peak maximum; thus the contribution of the background area to the overall value of β_i is larger for thinner coherent scattering domains.

(2) In the second test, Excel-calculated diffraction patterns for illite without PVP were compared with NEWMOD©-calculated illite patterns; Figure 1 is an example of such a comparison for illite having 0 Fe and 0.89 K per half unit-cell, and characterized by a lognormal distribution of coherent scattering domain size with $\bar{T}$ = 5 nm. The same correction for sample length as applied in NEWMOD© (*i.e.* 1° divergence slit, 20 cm goniometer, and 3.6 cm sample length) was used to correct the Excel calculated pattern. The similarity of the two theoretical diffraction tracings is satisfactory; small differences for 001 and 002 reflections probably result from a more complicated formulation of the LpG^2 factor used in NEWMOD© .

Table 4. Verification of the interference function calculation using lognormal coherent scattering domain thickness distributions with mean thicknesses of 5 nm and 10 nm. The measured integral breadth (β_i) of five illite reflections (position given in °2θ) is used to calculate the experimental mean volume-weighted thickness (L_{meas}). The theoretical value (L_{distr}) is calculated directly from the parameters of the lognormal distribution.

Reflection	°2θ	β_i	$\beta_i \cos\theta$ (rad)	L_{meas}	L_{distr}
$\bar{T}$ = 5 nm, lognormal distribution					
001	8.86	0.0254	0.0253	6.09	6.11
002	17.78	0.0256	0.0253	6.10	
003	26.8	0.0260	0.0253	6.09	
004	36	0.0266	0.0253	6.09	
005	45.44	0.0275	0.0253	6.09	
$\bar{T}$ = 10 nm, lognormal distribution					
001	8.86	0.0119	0.0119	13.00	13.11
002	17.78	0.0120	0.0118	13.02	
003	26.8	0.0122	0.0119	13.00	
004	36	0.0125	0.0119	13.00	
005	45.44	0.0128	0.0118	13.03	

RESULTS

Testing sample dispersion by PVP

XRD. The XRD effects of intercalation of the selected samples by PVP are compared to the glycolated samples in Figure 2. The *d*-values of the reflections (001, 002, 003 and 005) of all samples intercalated with PVP are shown in Table 1. The PVP-XRD patterns contain well-defined series of illite basal reflections, the spacings of which are related by *n* in Bragg's Law to that of the first-order reflection (9.98 Å). This is the basic criterion for confirming full dispersion of mixed-layer crystals by PVP (Eberl *et al.*, 1998b). In a few samples (M11, Zempleni, Ku-80, Ku-82, Jl4-16) d_{001} is too large for illite, whereas the positions of the remaining reflections correspond to those of illite. This displacement of the 001 is caused by interaction between the LpG^2 factor and broad interference functions for the peaks (Reynolds, 1980). When the LpG^2 factor is removed by division during MudMaster analysis, the d_{001} values decrease (Table 1, compare columns d_{001} and d_{001}int). In three cases, the 001 peaks of the interference function have not been satisfactorily extracted in MudMaster and the d_{001} values are too small (Zempleni and RW-1) or too large (Ku-80).

HRTEM. The results of applying the PVP technique in the imaging illite in HRTEM studies are very satisfactory. The HRTEM photographs of the Zempleni sample before (A) and after (B) intercalation with PVP are shown in Figure 3. The PVP-treated samples appear in HRTEM images as a collection of individual silicate layers (smectite monolayers) or sets of layers of strictly parallel orientation (illite crystals) with interlayer spacings of 10 Å. Smectite monolayers are abundant in the samples characterized by R = 0 ordering, whereas in R>0 illite-smectites, monolayers are scarce. Illite preserves its 10 Å spacing upon interaction with the resin as observed in several previous publications (*e.g.* Środoń *et al.*, 1990; Elsass *et al.*, 1998; Uhlik *et al.*, 2000b). The organization

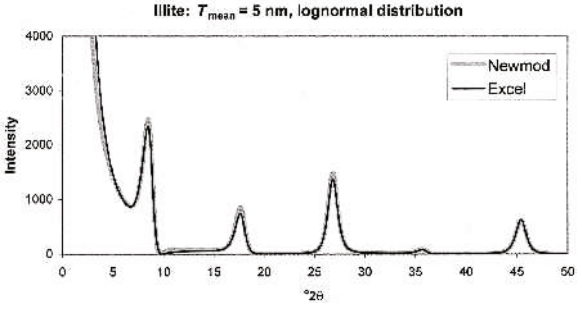

Figure 1. Illite diffraction patterns calculated using NEWMOD© computer program (Reynolds, 1985) and modeled in MS Excel®. The following parameters were applied for both calculations: lognormal crystal size distribution ($\bar{T}$ = 5 nm), Fe-free crystal structure and the correction for the intensity loss at low diffraction angles corresponding to the NEWMOD© default parameters.

https://doi.org/10.1346/000986002320679305 Published online by Cambridge University Press

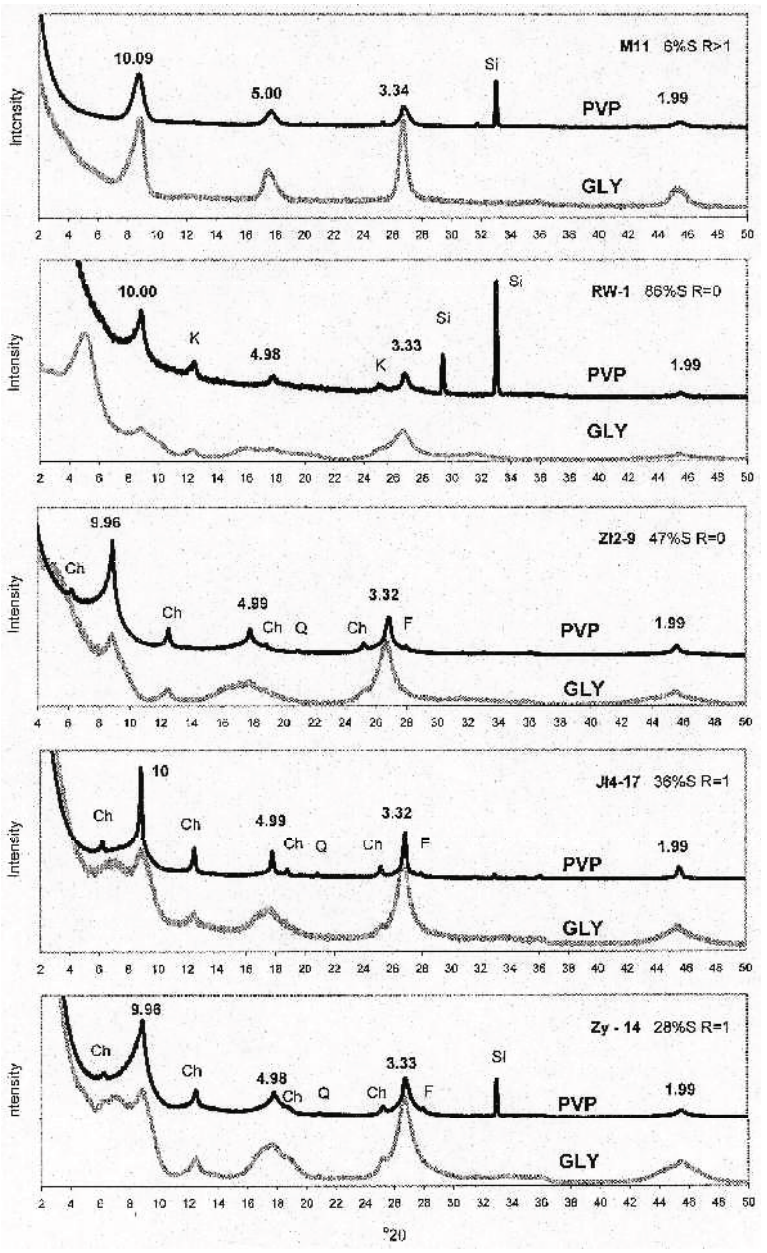

Figure 2. Examples of the XRD patterns of samples intercalated with PVP compared with glycolated samples (GLY) (intensities adjusted for presentation). *d*-values are given for the illite peaks in the profiles of the PVP-samples. Ch = chlorite, K = kaolinite, Q = quartz, F = feldspars, Si = a peak from Si wafer sample holder. All other peaks in the lower XRD-GLY pattern that do not correspond to the reflections in the upper XRD-PVP pattern belong to mixed-layer I-S, which becomes delaminated into fundamental particles in PVP preparations, giving the XRD characteristics of illite.

of crystals is not chaotic; they usually display approximately parallel orientation. The distances between the dispersed crystals are usually >10 nm; aggregated crystals comprise less than a few percent of the total mass of a sample. The thicknesses of illite crystals vary from two layers (bilayers) to >30 layers (very rare). Thick crystals (>10–15 layers), in contrast to thinner ones, sometimes exhibit stacking defects and splitting at the peripheries; they are usually blurred and their shapes are not well defined. The length of most crystals is variable and is not related to thickness, *i.e.* both thin (*e.g.* 2 layer) and thick (*e.g.* 15 layer) crystals may be either long or short. The length of the crystals was not taken into account in the present study, because it might be an imaging artifact due to the curved shape of the crystals. Whereas bentonitic samples are composed exclusively of smectite and illite crystals, shales also contain some 14 Å crystals which were interpreted as chlorite (similar to that observed by Vali and Köster, 1986; Środoń *et al.*, 1990; Elsass *et al.*, 1998). The number of crystals measured by HRTEM in

https://doi.org/10.1346/000986002320679305 Published online by Cambridge University Press

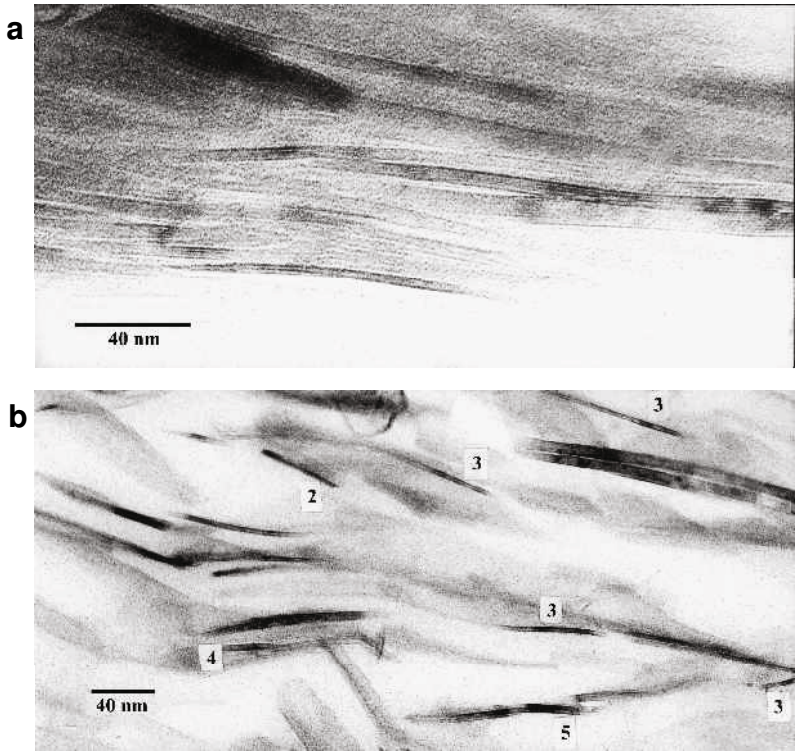

Figure 3. HRTEM image of Zempleni bentonite before (a) and after (b) intercalation with PVP. The number of layers are given near the crystals in b.

sample JŁ4-13 is statistically invalid, due to unsuccessful sample preparation (Table 5).

XRD vs. HRTEM measurements of illite crystal thickness distribution

A comparison between illite coherent scattering domain thickness distributions measured by the XRD and crystal thickness distributions measured by HRTEM is presented in Figure 4 and in Table 5. The table includes values of $\bar{T}$ evaluated by the two techniques, lognormal parameters α and β^2 (Drits *et al.*, 1998), percentage of smectite monolayers calculated from HRTEM images, and total number of crystals counted on HRTEM images (n). In the following analysis,

Table 5. Basic parameters of particle thickness distributions measured by XRD and HRTEM: mean thickness ($\bar{T}$), distribution parameters (α and β^2) (for strict comparison with XRD, the HRTEM parameters are calculated for distributions without smectite monolayers), % of monolayers in the samples as estimated by the HRTEM method, and number of particles measured by HRTEM: including monolayers (N_{I+S}), and excluding monolayers (N_{Illite}).

Sample	$\bar{T}_{XRD}$	$\bar{T}_{HRTEM\ (Illite)}$	α_{XRD}	$\alpha_{HRTEM\ (Illite)}$	β^2_{XRD}	$\beta^2_{HRTEM\ (Illite)}$	% monolayers	N_{I+S}	N_{Illite}
Ku-80	3.8	3.2	1.18	1.05	0.26	0.18	35.0	425	277
Ku-82	4.5	4.1	1.36	1.26	0.28	0.25	1.8	393	386
JŁ4-13	4.0	3.1	1.16	1.05	0.29	0.15	35.0	52	34
JŁ4-16	3.8	3.4	1.18	1.06	0.26	0.24	40.0	402	241
JŁ4-17	4.4	3.1	1.21	1.02	0.38	0.17	1.0	551	545
ZŁ2-6	3.6	3.7	1.12	1.14	0.26	0.26	62.0	416	156
ZŁ2-9	3.9	3.2	1.17	1.03	0.31	0.22	50.0	612	304
ZŁ2-12	4.2	3.2	1.22	0.99	0.33	0.22	12.0	515	452
ZŁ2-14	4.1	3.5	1.21	1.10	0.29	0.23	9.0	293	267
RW-1	3.5	3.1	1.09	1.00	0.26	0.18	63.0	780	285
Zy-28	3.7	3.2	1.11	1.05	0.30	0.19	1.2	420	415
Zy-19	3.8	4.6	1.16	1.38	0.27	0.23	0.6	489	486
Zy-14	4.0	3.5	1.22	1.15	0.27	0.19	0.0	682	682
RM30	12.7	9.2	2.39	2.09	0.30	0.27	0.0	238	238
M11	6.8	6.5	1.78	1.75	0.29	0.22	0.0	440	440
Zemp	4.4	3.8	1.42	1.28	0.14	0.11	0.0	315	315

https://doi.org/10.1346/000986002320679305 Published online by Cambridge University Press

coherent scattering domains and crystals are collectively referred to as 'particles'. Thicker particles are usually much less abundant than thinner ones, and are hardly visible in size-frequency diagrams when all thickness classes are treated graphically in the same way. Therefore in Figure 4, the frequencies of thicker particles are multiplied by a factor of 10 (30 for Zempleni). The multiplication starts at the 11 nm thickness class for shale samples and for Zempleni, at 17 nm for M11, and at 32 nm for RM30 (to the right of the vertical dashed lines). For the shale samples the following observations were made (Figure 4a):

(1) Both techniques usually detect the same mode.

(2) X-ray diffraction detects a larger fraction of the thick and smaller fraction of the thin particles as compared to the distributions obtained by the HRTEM. This results in larger $\bar{T}$ and larger α and β^2 for the XRD measurements (Table 5).

(3) Up to ~10 nm, both HRTEM and XRD distributions are smooth and their shapes are similar; but for thicker particles, significant differences in size-frequency data exist between the two techniques: the two profiles match poorly and the HRTEM distributions are scattered.

(4) The maximum thickness classes (T_{max}) measured by XRD and HRTEM techniques are different for different samples and do not show any systematic pattern. The T_{max} of XRD distributions range from 18 nm (RW-1) to 50 nm (Zł2-14, Zy-19), whereas those for HRTEM distributions range from 8 nm (Jł4-13) to 40 nm (Zy-19). The HRTEM measurements, however, show only a few 30–40 nm particle classes (Zł2-12, Zł2-14, Zy-19, Ku-82), whereas XRD detects a considerably larger number of thick particle classes (RM30, Jł4-17, Zł2-9, Zł2-12, Zł2-14, Zy-28).

The differences between the XRD and HRTEM data seem attributable to differences between number- and area-weighted distributions. To test this hypothesis, the PVP-XRD and PVP-HRTEM results for the bentonitic samples of the present study are compared with Pt-shadowing TEM measurements of Środoń *et al.* (2000), which were performed on the same samples (Figure 4b). Both number-weighted (nw) and area-weighted (aw) distributions were taken from Środoń *et al.* (2000) in order to make a direct comparison between HRTEM and XRD measurements. Area-weighted distributions measured by the Pt-shadowing TEM technique for the bentonitic samples do not fit the XRD data better than the number-weighted HRTEM or TEM distributions.

Verification of the two techniques by comparing theoretical and experimental illite diffraction patterns

The theoretical diffraction patterns were calculated as described above for two bentonitic samples (Zempleni and M11) and for four shale samples (Zł2-6, Zł2-9, Zy-14, Jł4-17) (Figure 5). This experiment assumes that the illite crystals seen in HRTEM are equivalent to coherent scattering domains (an assumption supported by Eberl *et al.*, 1998b, and confirmed in the present study, see below). For the HRTEM distributions, diffraction patterns were calculated both excluding and including monolayers. Monolayers scatter X-rays but do not contribute to diffraction peaks, thus their presence is not registered by the interference function (for monolayers $\phi = 1$) but they affect the shape of the background, raising it at low angles. For bentonites, the Pt-shadowing TEM data (area-weighted distributions) of Środoń *et al.* (2000) were also used. The number-weighted HRTEM distributions were recalculated to represent the area-weighted distributions, using regression equations established for lognormal distributions by Środoń *et al.* (2000, Figure 4). This correction could not be applied to shales, because their illite particle thickness distributions are not lognormal. Shale samples were selected for modeling according to two criteria: the type of ordering, and the degree of similarity between XRD and HRTEM distributions. Among R = 0 clays, Zł2-6 and Zł2-9 represent the two extremes, the former has the best, and the latter the worst fit between XRD and HRTEM distributions. Similarly, Zy-14 and Jł4-17 were selected among the samples characterized by R = 1 ordering.

A direct comparison between diffraction patterns calculated using various crystal size distributions requires the background function to be taken into account; this is present in the experimental XRD tracings, but is not included in the theoretical calculations. The shape of background for PVP clays has not been determined theoretically. In the present study, it was approximated by an XRD pattern of a sample having 10 mg PVP on a Si substrate. The comparison requires normalization of intensities, because theoretically calculated patterns are in arbitrary units, whereas experimental diffraction patterns are expressed in counts per second (cps). Also, the experimentally determined background needs to be normalized to the PVP diffraction patterns. Therefore, the patterns were treated as follows:

(1) First, the PVP background pattern was adjusted by trial and error to fit the experimental PVP illite pattern. This fit was usually accomplished by normalization of the smallest background intensities to the smallest intensities of the illite pattern; this treatment required only a slight reduction of the background intensities because both the PVP on the Si substrate and the PVP-samples were run under similar conditions.

(2) In the second step, the normalized background was subtracted from the experimental illite pattern (Figure 6).

(3) Finally, the theoretical XRD patterns, calculated using both XRD and microscopic measurements, were normalized to the 001 reflection of the experimental PVP diffractogram without the background. Normalization to 001 peak was chosen in all cases, because the XRD-derived illite crystal thickness distribution, which

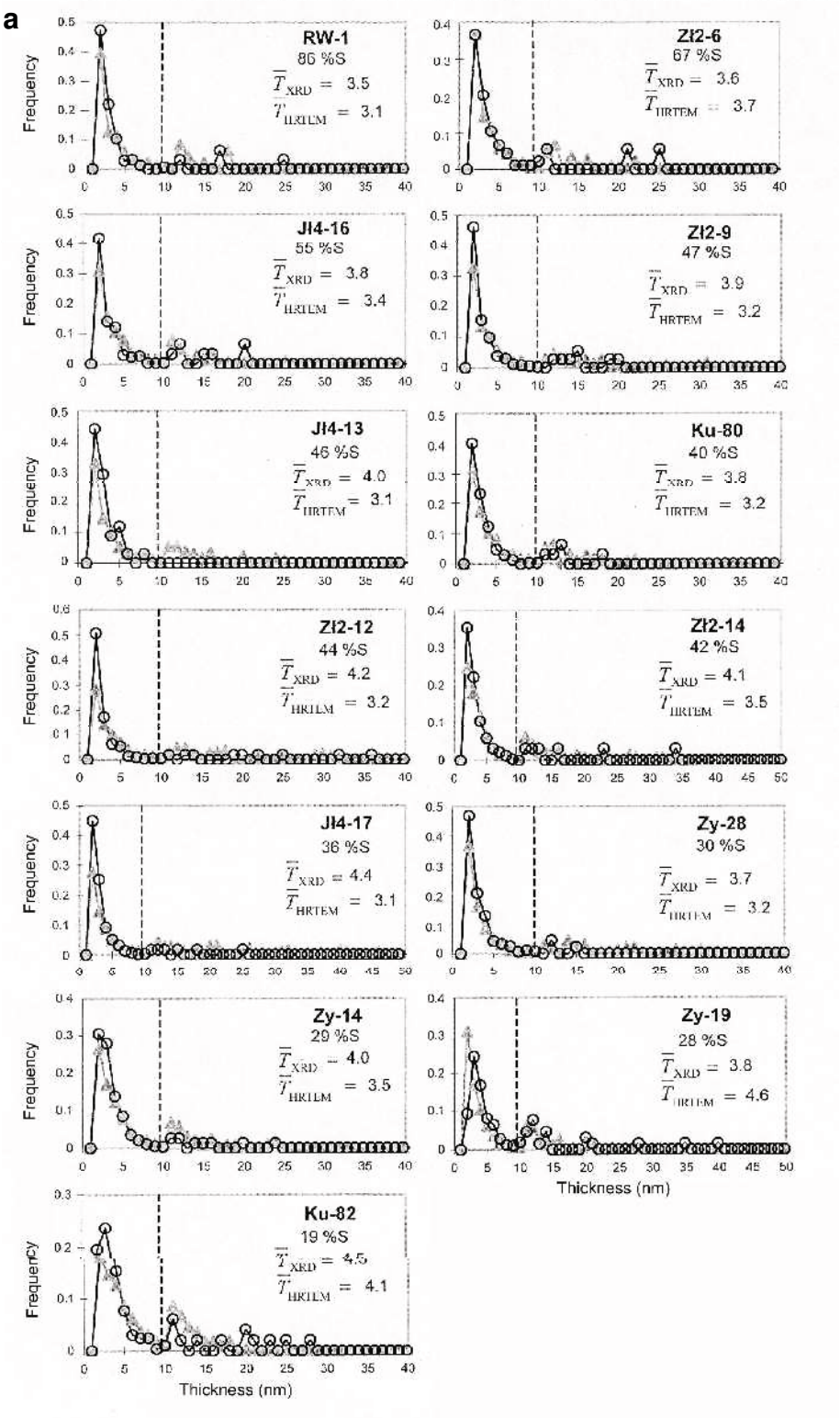

Figure 4. Comparison between XRD (triangles) and HRTEM (circles) illite particle thickness distributions for shales (a) and bentonites (b) (*facing page*). The samples in the two sets are arranged according to the decreasing expandability. Mean thicknesses are given in nm. The XRD and HRTEM distributions for bentonites are compared with Pt-shadowing TEM data (Środoń *et al.*, 2000), both number-weighted (squares) and area-weighted (diamonds). In order to be able to observe the distribution of thicker particles, their frequencies were multiplied by 10 (and 30 for Zempleni) to the right of the vertical line.

https://doi.org/10.1346/000986002320679305 Published online by Cambridge University Press

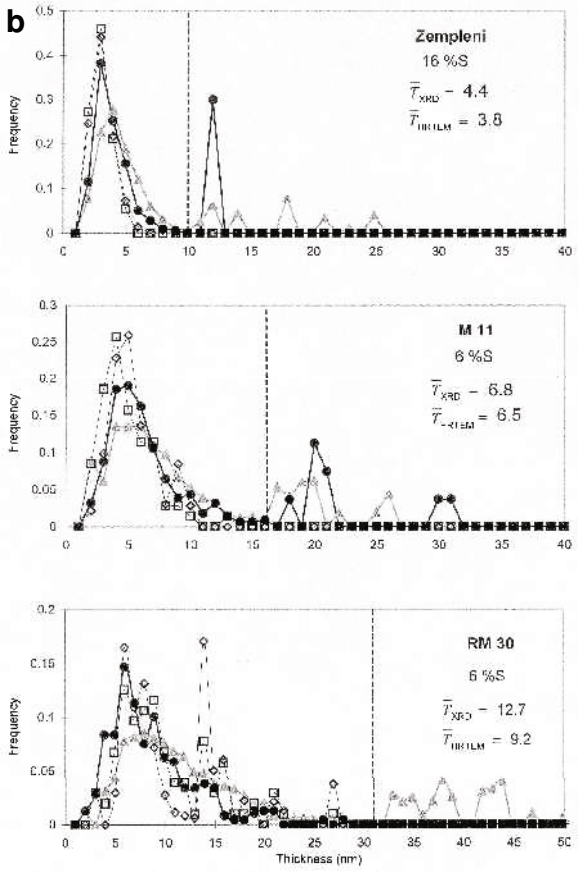

Figure 4. (*contd.*)

was used to create the theoretical function, was based on this reflection. The 003, 004 and 005 reflections of experimental diffraction patterns were not suitable for a direct comparison because the intensity of the 003 peak contained interference from quartz, the 004 was usually too small and difficult to detect, and 005 suffered from intensity loss due to insufficient thickness of the PVP preparations (their very small mean absorption coefficient requires large thickness to fulfil the infinite thickness criterion, (Moore and Reynolds, 1997, p. 302)). In order to make Figure 5 more readable, only the 001, 002 and 003 reflections are shown.

Bentonites (Figure 5a,b). For bentonites, all theoretical patterns match the experimental data relatively well. The patterns calculated using XRD particle thickness distributions match the experimental patterns best (both peak positions and broadening); however, a 4–8°2θ valley and the intensities of the 003 and 005 reflections (the latter is not shown) cannot be fitted precisely. A slight improvement in the low-angle region was obtained for the Zempleni sample by the modification of LpG^2 factor, by applying a larger proportion of $(\mathrm{Lp}G^2)_{\mathrm{PVP\text{-}smectite}}$: $(\mathrm{Lp}G^2)_{\mathrm{illite}}$ than would result from the mean thickness of particles (equation 1), thereby increasing the effect of edges on overall LpG^2 (see below). The XRD pattern calculated using the LpG^2 factor modified in this way is presented in Figure 7 (black solid line). Worse fits to the experimental profiles were obtained when the theoretical diffraction patterns were calculated using the microscopic distributions. The HRTEM data better simulate the experimental XRD patterns than TEM-measured area-weighted distributions. Number- and area-weighted HRTEM distributions produce similar results.

R = 1 shales (Figure 5c,d). As for the bentonites, the theoretical patterns calculated using the XRD distributions match the experimental patterns better than if the HRTEM distributions are used, although the 4–8°2θ valley, the widths of the 002, 003 and 005 peaks and the intensities of the 003 and 005 reflections show some misfit. The fit for XRD data can be improved remarkably by applying wider distributions, *i.e.* a distribution not limited by the MudMaster criterion that the mean thickness from the distribution has to be equal to the extrapolated (best) mean (see above). For Jł4-17, the criterion is fulfilled when the distribution is limited at 47 nm (gray line), whereas the best fit is obtained when the distribution is increased to the 60 nm thickness class (black line). For Zy-14, the difference is smaller: 30 nm instead of 28 nm. The maximum thickness class was assessed by trial and error. Theoretical patterns simulated with HRTEM-measured distributions produce a considerably worse fit to experimental profiles. There are only a few monolayers in the R = 1 samples (Table 5), thus the differences between the patterns calculated using the 'I+S' and 'Illite' distributions are negligible, and only the former are shown in the figure.

R = 0 shales (Figure 5e,f). For Zł2-6, for which both XRD and HRTEM produce similar distributions, the best fit was obtained when a theoretical pattern was calculated with HRTEM distribution including monolayers (see Table 5). When monolayers were excluded, the fit was worse for the 001 reflection and the pattern became similar to that calculated from the XRD distribution. For Zł2-9, XRD-based distribution simulates the experimental pattern slightly better (especially for 002 and 003) than HRTEM-based calculations; however, none of the theoretical patterns produces a satisfying fit.

INTERPRETATION AND DISCUSSION

Comments on testing the dispersion of mixed-layer crystals by PVP

As shown in Table 1, the majority of the PVP samples fulfil the main condition for complete dispersion of mixed-layer crystals into fundamental particles, *i.e.* they produce the rational series of the d_{00l} spacings. For broad 001 reflections, which may be shifted by the LpG^2 factor, the *d*-values of the extracted interference

https://doi.org/10.1346/000986002320679305 Published online by Cambridge University Press

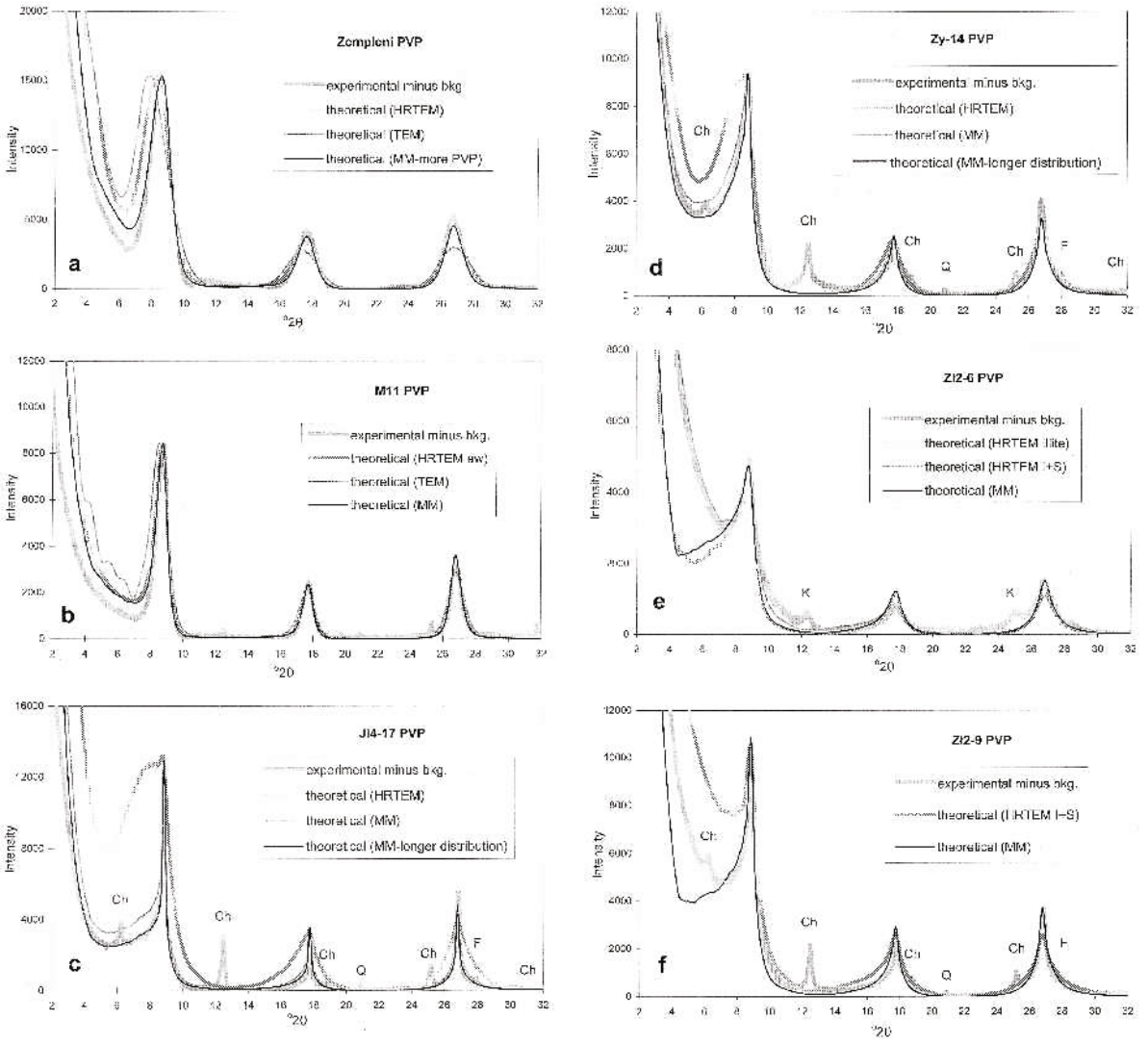

Figure 5. Verification of experimentally-determined distributions for bentonites (a and b), R = 1 shales (c and d), and R = 0 shales (e and f). Experimental XRD patterns of samples intercalated with PVP (with background removed as shown in Figure 6) are modeled with theoretical diffraction functions of illite calculated in MS Excel using distributions determined by the XRD, HRTEM and Pt-shadowing TEM techniques. Ch = chlorite, K = kaolinite, Q = quartz, F = feldspars.

function should be taken into account. However, the d_{001} values of the extracted interference function for Zempleni and RW-1, characterized by relatively broad first-order reflections, are too small and are unacceptable. It was shown (Dudek, 2001) that differences between the actual amount of PVP in a sample and that assumed in MudMaster on the basis of the mean thickness of coherent scattering domains (equation 1) will affect the position of the 001 peak of the extracted interference function (especially for broad peaks). The positions of the 002, 003, 004 and 005 peaks remain unaffected. Excess PVP in a sample relative to the amount assumed in MudMaster will shift the 001 peak of the extracted interference function towards larger angles, thus lowering *d*-values, as for Zempleni and for RW-1. The $\mathrm{Lp}G^2$ factor used in MudMaster to study Zempleni and RW-1 can be corrected by decreasing the proportion $(\mathrm{Lp}G^2)_{\mathrm{illite}}$:$(\mathrm{Lp}G^2)_{\mathrm{PVP\text{-}smectite}}$. The results presented in Table 6 indicate that such treatment leads to a considerable and satisfactory improvement of d_{001} with only slight modification of the resulting distribution. Moreover, the theoretical XRD pattern calculated using the corrected ratio of $\mathrm{Lp}G^2_{\mathrm{illite}}$:$\mathrm{Lp}G^2_{\mathrm{PVP\text{-}smectite}}$, produces a better fit (though not perfect) than does the theoretical pattern without this correction (Figure 7). Therefore PVP in the sample may disturb the relation between the position of 001 reflection and those of the higher orders. Thus, it is safer to rely on the *d*-values of 002 and the higher-order reflections as the main test for a complete intercalation of samples by PVP (compare Table 1).

The most reliable evidence for the total dispersion of I-S mixed-layer crystals into fundamental particles

https://doi.org/10.1346/000986002320679305 Published online by Cambridge University Press

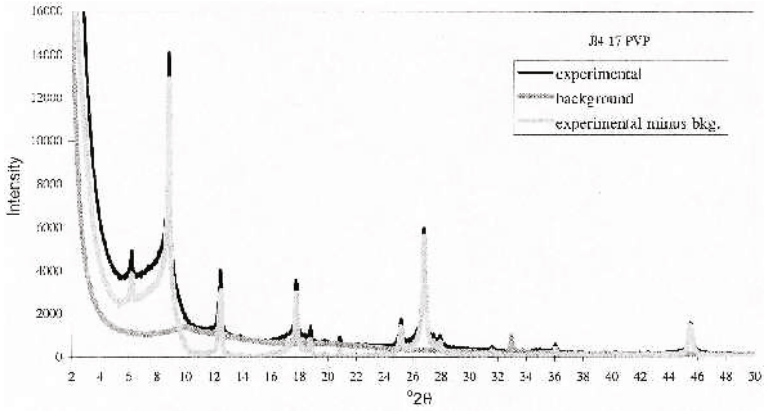

Figure 6. The result of subtraction (light gray line) of experimentally determined background for PVP clays (XRD pattern of 10 mg PVP on the Si substrate, dark gray line) from the experimental pattern of a sample intercalated with PVP (black line). The XRD patterns obtained in this way (denoted as experimental minus bkg) were modeled as shown in Figure 5.

comes from direct inspection of HRTEM micrographs. In the majority of pictures, fundamental particles are well dispersed and far enough from each other (usually ~5–10 nm) to prevent interparticle diffraction effects.

Interpretation of differences between XRD and HRTEM measurements

The results of theoretical modeling of experimental XRD patterns of PVP samples offer independent proof of the high degree of accuracy of the BWA measurements of crystal thickness distribution. For the bentonitic samples characterized by R>1 ordering, computer simulations which apply the XRD distributions fit the experimental patterns well. This fit can sometimes be improved by modifying $Lp G^2$ by adding more PVP. The small misfit in the 4–8°2θ range may be related to some error in the selected shape of the background, which was adjusted by trial and error to the theoretically calculated patterns. For the shale R = 1 samples, this misfit can be removed and an almost perfect fit with the experimental patterns can be obtained by using a wider distribution

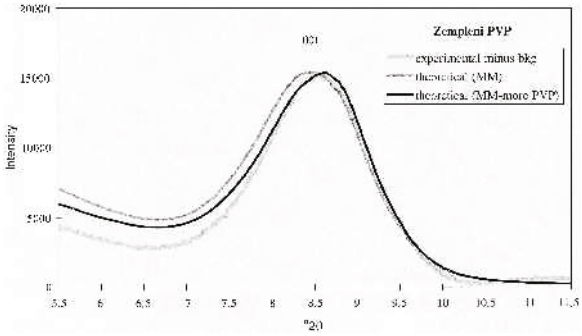

Figure 7. Modeling of 001 reflection of Zempleni-PVP using XRD-determined distribution. The figure shows in detail the differences between theoretical patterns resulting from applying different $Lp G^2$ factors. The gray line represents the standard case, *i.e.* $Lp G^2$ factor is calculated from equation 1. The fit is improved however, when the $Lp G^2$ factor is modified by applying a higher proportion of $(Lp G^2)_{PVP\text{-}smectite}$:$(Lp G^2)_{illite}$ than would result from the mean thickness value.

than the standard one suggested in MudMaster. Thus, the simulation of theoretical XRD patterns can be used as a method to verify and improve the MudMaster results by using the best-fit criterion instead of an arbitrary cut-off of the Fourier coefficients series. As shown in Table 5, the microscopic methods, in the majority of cases, underestimate the mean thickness compared to the XRD technique.

If Figure 4 is modified so that the frequencies of the whole population of particles are split into two thickness fractions, $\leqslant$10 nm and >10 nm, and then the frequencies are normalized separately to 1 (Figure 8), the fit of the XRD and HRTEM data for the thinner particles is very good and the fit for the thicker fraction is poor. This calculation indicates that the major source of discrepancy between XRD and HRTEM distributions is related to the underestimation of the contributions of thicker particles by HRTEM. This underestimation comes from inaccurate counting statistics for thick crystals, and the availability of number-weighted distributions, in contrast to the area-weighted distributions registered by XRD. Thicker illite crystals have bigger areas and this relationship is exponential (Środoń *et al.*, 2000); therefore, the contribution of thick crystals to XRD area-weighted distributions is larger than if they are weighted by the number and this effect increases with crystal thickness.

For the bentonitic samples characterized by lognormal distributions, correction of the microscopic data for the area-weighted distributions is not very important for samples with relatively small $\bar{T}$, such as those used in this study (Figure 4b). For shales, this factor may be of great importance, even for samples of relatively small $\bar{T}$, because the size distributions of illite crystals in shales are more diverse than those in bentonites due to the presence of thicker detrital micas. For example, R = 1 shale sample JH4-17 in Figure 4a clearly shows that the XRD technique identifies very thick crystals (up to 46 nm), which were not observed by HRTEM. Such thick crystals have large areas and contribute more

https://doi.org/10.1346/000986002320679305 Published online by Cambridge University Press

Table 6. The effect of varying LpG^2 factor used in MudMaster on the parameters of distribution ($\bar{T}$, α, β^2) and d_{001} values of the extracted interference function for samples Zempleni and RW-1. The differences between LpG^2 factors were obtained by applying different illite:PVP-smectite ratios. Original: $LpG^2_{PVP\text{-}illite}$ resulting from $\bar{T}$ of the distribution, as calculated by MudMaster (equation 1); Corrected: $LpG^2_{PVP\text{-}illite}$ having a lower proportion of crystal interiors (represented by LpG^2 of illite) to crystal edges (represented by LpG^2 of smectite intercalated with PVP). See text for details.

	$(LpG^2)_{illite}$:$(LpG^2)_{PVP\text{-}smectite}$	$\bar{T}$	α	β^2	d_{001}
Zempleni	Original: 0.77	4.4	1.42	0.14	9.85
	Corrected: 0.71	4.5	1.43	0.16	9.98
RW-1	Original: 0.71	3.5	1.09	0.26	9.91
	Corrected: 0.67	3.6	1.09	0.29	9.96

strongly to the overall frequencies than if weighted by numbers. These factors produce a considerable difference between $\bar{T}$ obtained from the two techniques. Therefore theoretical modeling of JŁ4-17 yields poor results if the HRTEM distribution is applied (Figure 5c). For the other R = 1 shale sample, Zy-14, the XRD and HRTEM distributions and the values of $\bar{T}_{XRD}$ and $\bar{T}_{HRTEM}$ are not as disparate. The simulation of the diffraction pattern of Zy-14 using the microscopic data produces better fit than for JŁ4-17; yet it is not very good because $\bar{T}_{XRD} > \bar{T}_{HRTEM}$. Similar differences between $\bar{T}_{XRD}$ and $\bar{T}_{HRTEM}$ and the degree of fit between the XRD- and HRTEM-based theoretical diffraction patterns exist for the bentonitic sample Zempleni. In contrast, M11 is characterized by similar values of $\bar{T}_{XRD}$ and $\bar{T}_{HRTEM}$, and both XRD and HRTEM distributions used in calculation of theoretical patterns produce equally good results.

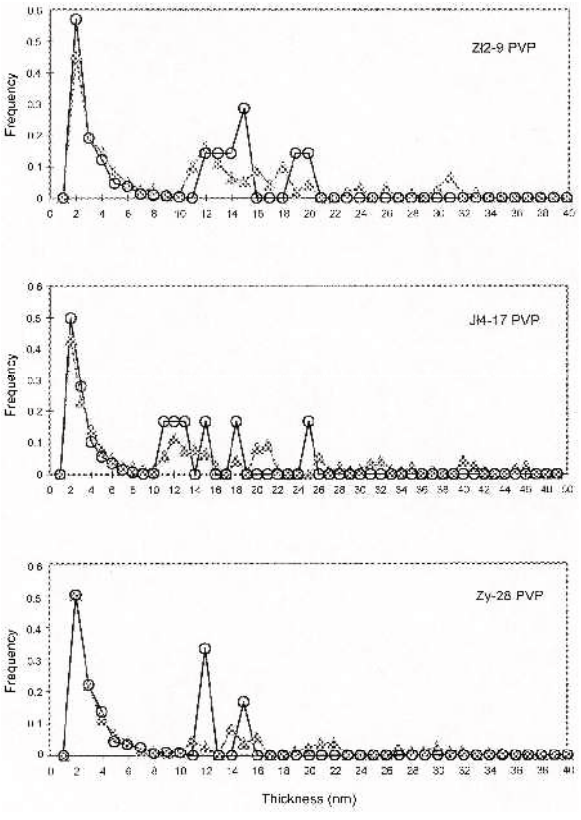

Figure 8. Comparison of the distributions determined by XRD (triangles) and HRTEM (circles) normalized separately to 1 for the finer ($\leqslant$10 nm) and the coarser (>10 nm) fractions of particles.

For the shale samples characterized by R = 0 ordering, the XRD distributions are incomplete, because they do not contain smectite monolayers, which comprise a considerable proportion of these samples (Table 5). Therefore theoretical patterns fail to simulate the low-angle region of the experimental diffraction patterns. In the case of R = 0 illite-smectites, the microscopic techniques have the advantage over MudMaster, because they can detect smectite monolayers. However, a precise fitting of the pattern calculated with the HRTEM 'I+S' distribution can be obtained only if $\bar{T}_{HRTEM\ (Illite)}$ is approximately equal to $\bar{T}_{XRD}$, *i.e.* if the HRTEM and XRD distributions are similar such as they are for shale sample ZŁ2-6 (Figure 5e). When this condition is not fulfilled, such as for sample ZŁ2-9 (Figure 5f), neither XRD nor HRTEM distributions give good results, the former because of failure to take into account smectite monolayers, and the latter because the thicker illites are underestimated.

Uhlik *et al.* (2000a) compared the XRD (MudMaster) and the HRTEM distributions of pyrophyllite crystal thicknesses. They obtained similar results to those presented in this work: HRTEM calculations overestimated thin and underestimated thick crystals, and the differences between the two techniques were exaggerated for samples having large mean thicknesses.

The BWA technique was applied by a number of authors (Lanson and Kübler, 1994; Árkai *et al.*, 1996; Warr and Nieto, 1998) to study size and size distributions of phyllosilicates from low-temperature metamorphic pelites, which are commonly characterized by crystal thickness >20 nm. The authors showed that the XRD means were usually underestimated compared with the microscopic measurements. This relationship, opposite to that established in the present study, may reflect the effect of instrumental broadening of XRD peaks for samples containing thick crystals.

https://doi.org/10.1346/000986002320679305 Published online by Cambridge University Press

Coherent scattering domains vs. fundamental particles

The good fit of the HRTEM and XRD distributions for thin illite particles (Figure 8) is reliable evidence that illite particles measured in HRTEM are equivalent to the coherent scattering domains, which are the entities analyzed by XRD. This conclusion confirms the observations of Eberl *et al.* (1998b). The considerably worse fit for the thicker fraction is a result of imprecise statistics.

CONCLUSIONS

(1) The full dispersion of mixed-layer I-S crystals by PVP in the studied samples has been confirmed by detailed investigation of HRTEM micrographs and by analyzing the positions of XRD basal reflections. In HRTEM micrographs, crystal thicknesses can be measured simply by counting the number of layers.

(2) Two independent techniques for crystal size distribution measurements, XRD and HRTEM, were compared by analyzing the thickness of illite crystals in several samples of bentonites and shales (from the zone of diagenesis) treated with PVP. The XRD technique (MudMaster), which gives area-weighted distributions, detects a larger proportion of thick crystals than does HRTEM, which produces number-weighted distributions. As a result, $\bar{T}$, α and β^2 are usually larger for the former. For the fine fraction of illite crystals (<10 nm), both techniques produce similar thickness distributions.

(3) The reliability of the two techniques was evaluated by using illite crystal thickness distributions obtained from the two methods to simulate experimental diffraction patterns of PVP illites. These tests proved that the distributions measured by XRD are very accurate. The fits between the experimental and modeled profiles can be improved further if the range of thickness classes applied in modeling is extended beyond that required to fulfil the MudMaster criterion ($\bar{T}$ from the distribution equals extrapolated $\bar{T}$). Thus, the modeling of the experimental XRD patterns of PVP-illites, applied in the present study, can be used as a tool to correct the MudMaster analysis. Underestimation of the proportion of thick crystals by HRTEM (especially >15 nm) leads to considerable misfit between experimental XRD pattern and the theoretical profile calculated using the HRTEM data.

(4) The collected data indicate that crystals measured by HRTEM are equivalent to the coherent scattering domains analyzed by XRD in PVP preparations.

ACKNOWLEDGMENTS

This paper reports part of the PhD thesis of Teresa Dudek directed by Jan Środoń. Most of the microscopic part of the study was realized within the framework of the French-Polish scientific cooperation. The authors thank Mrs Małgorzata Buś, Mrs Małgorzata Zielińska, Mr Jean Lapeyronnie and Mrs Maria Čaplovičova for their technical assistance. Thorough reviews by Dr G.R. Thompson and Dr L. Warr helped to improve the clarity of the manuscript.

REFERENCES

Árkai, P., Merriman, R.J., Roberts, B., Peacor, D.R. and Tóth, M. (1996) Crystallinity, crystallite size and lattice strain of illite-muscovite and chlorite: comparison of XRD and TEM data for diagenetic to epizonal pelites. *European Journal of Mineralogy,* **8**, 1119–1138.

Drits, V., Środoń, J. and Eberl, D.D. (1997) XRD measurement of mean crystallite thickness of illite and illite/smectite: reappraisal of the Kübler index and the Scherrer equation. *Clays and Clay Minerals,* **45**, 461–475.

Drits, V., Eberl, D.D. and Środoń, J. (1998) XRD measurement of mean thickness, thickness distribution and strain for illite and illite-smectite crystallites by the Bertaut-Warren-Averbach technique. *Clays and Clay Minerals,* **46**, 38–50.

Dudek, T. (2001) Diagenetic evolution of illite-smectite in the Miocene shales from the Przemyśl area (Carpathian Foredeep). PhD thesis, Institute of Geological Sciences, Polish Academy of Sciences, 155 pp.

Eberl, D.D., Środoń, J., Lee, M., Nadeau, P.H. and Northrop, H.R. (1987) Sericite from the Silverton caldera, Colorado: Correlation among structure, composition, origin and particle thickness. *American Mineralogist,* **72**, 914–934.

Eberl, D.D., Drits, V.A., Środoń, J. and Nuesch, R. (1996) MUDMASTER: A program for calculating crystallite size distributions and strain from the shapes of X-ray diffraction peaks. *U.S. Geological Survey, Open-File Report 96-171.*

Eberl, D.D., Drits, V. and Środoń, J. (1998a) Deducing growth mechanisms for minerals from the shapes of crystal size distributions. *American Journal of Science,* **298**, 499–533.

Eberl, D.D., Nuesch, R., Šucha, V. and Tsipursky, S. (1998b) Measurement of fundamental illite particle thicknesses by X-ray diffraction using PVP-10 intercalation. *Clays and Clay Minerals,* **46**, 89–97.

Elsass, F., Beaumont, A., Pernes, M., Jaunet, A-M. and Tessier, D. (1998) Changes in layer organization of Na- and Ca- exchanged smectite materials during solvent exchanges for embedment in resin. *The Canadian Mineralogist,* **36**, 1475–1483.

Jackson, M.L. (1975) *Soil Chemical Analysis – Advanced Course* (M. Jackson editor). University of Wisconsin, Madison, USA.

Kile, D.E., Eberl, D.D., Hoch, A.R. and Reddy, M.M. (2000) An assessment of calcite crystal growth mechanism based on crystal size distributions. *Geochimica et Cosmochimica Acta,* **64**, 2937–2950.

Lanson, B. and Kübler, B. (1994) Experimental determination of coherent scattering domain size distribution of natural mica-like phases with the Warren-Averbach technique. *Clays and Clay Minerals,* **42**, 489–494.

Merriman, R.J., Roberts, B. and Peacor, D.R. (1990) A transmission electron microscope study of white mica crystallite size distribution in a mudstone to slate transitional sequence, North Wales, UK. *Contributions to Mineralogy and Petrology,* **106**, 27–40.

Moore, D.M. and Reynolds, R.C., Jr. (1997) *X-ray Diffraction and the Identification and Analysis of Clay Minerals.* Oxford University Press, New York.

Nadeau, P.H., Tait, J.M., McHardy, W.J. and Wilson, M.J. (1984) Interstratified XRD characteristics of physical mixtures of elementary clay particles. *Clay Miner*als, **19**, 67–76.

Nieto, F. and Sanchez-Navas, A. (1994) A comparative XRD and TEM study of the physical meaning of the white mica

'crystallinity' index. *European Journal of Mineralogy,* **6**, 611–622.

Reynolds, R.C., Jr. (1980) Interstratified clay minerals. Pp. 249–304 in: *Crystal Structures of Clay Minerals and their X-ray Identification* (G.W. Brindley and G. Brown, editors). Monograph **5**. Mineralogical Society, London.

Reynolds, R.C., Jr. (1985) *NEWMOD*© a computer program for the calculation of one-dimensional diffraction patterns of mixed-layered clays. R.C. Reynolds, 8 Brook Dr., Hanover, New Hampshire, USA.

Spurr, A.R. (1969) A low viscosity epoxy resin embedding medium for electron microscopy. *Journal of Ultrastructural Research,* **26**, 31–43.

Środoń, J. (1984) X-ray powder diffraction identification of illitic materials. *Clays and Clay Minerals,* **32**, 337–349.

Środoń, J., Morgan, D.J., Eslinger, E.V., Eberl, D.D. and Karlinger, M.R. (1986) Chemistry of illite/smectite and end-member illite. *Clays and Clay Minerals,* **34**, 368–378.

Środoń, J., Andreoli, C., Elsass, F. and Robert, M. (1990) Direct high-resolution transmission electron microscopic measurements of expandability of mixed-layer illite/smectite in bentonite rock. *Clays and Clay Minerals,* **38**, 373–379.

Środoń, J., Eberl, D.D. and Drits, V. (2000) Evolution of fundamental particle size during illitization of smectite and implications for the illitization mechanism. *Clays and Clay Minerals,* **48**, 446–459.

Tessier, D. (1984) Etude experimentale de l'organisation des materiaux argileux. Dr Science thesis, University of Paris VII, Paris, INRA publisher, pp. 125–130.

Uhlik, P. (1999) Evolution of illite-smectite particles during diagenesis. PhD thesis, Comenius University, 101 pp. (in Slovak).

Uhlik, P., Šucha, V., Eberl, D.D., Puskelova, L. and Čaplovičova, M. (2000a) Evolution of pyrophyllite particle sizes during dry grinding. *Clay Minerals,* **35**, 423–432.

Uhlik, P., Šucha, V., Elsass, F. and Čaplovičova, M. (2000b) High-resolution transmission electron microscopy of mixed-layer clays dispersed in PVP-10: A new technique to distinguish detrital and authigenic illitic material. *Clay Minerals,* **35**, 781–789.

Vali, H. and Köster, H.M. (1986) Expanding behaviour, structural disorder, regular and random irregular interstratification of 2:1 layer-silicates studied by high-resolution images of transmission electron microscopy. *Clay Minerals,* **21**, 827–859.

Warr, L.N. and Nieto, F. (1998) Crystallite thickness and defect density of phyllosilicates in low-temperature metamorphic pelites: a TEM and XRD study of clay mineral crystallinity index standards. *The Canadian Mineralogist,* **36**, 1453–1474.

(*Received 20 November 2001; revised 15 March 2002; Ms. 606; A.E. Douglas K. McCarty*)